Татьяна Витальевна Бедыч* – техника ғылымдарының кандидаты, энергетика және машина жасау кафедрасының қауымдастырылған профессоры, М.Дулатов атындағы Қостанай инженерлік-экономикалық университеті, Қазақстан Республикасы; e-mail: tbedych@mail.ru. ORCID: https://orcid.org/0000-0003-3642-8917.

Максат Амантайулы Амантаев – PhD, аграрлық техника және көлік кафедрасының қауымдастырылған профессоры, «Ахмет Байтұрсынұлы атындағы Қостанай өңірлік университеті» КЕАҚ, Қазақстан Республикасы; e-mail: amantayev.ma@ksu.edu.kz. ORCID: https://orcid.org/0000-0002-4838-9487.

Риза Ғабдысалық – PhD, «Postgraduate» секторының қауымдастырылған профессоры, Д.Серікбаев атындағы Шығыс Қазақстан техникалық университеті, Қазақстан Республикасы; e-mail: riza.gabdyssalyk@mail.ru. ORCID: https://orcid.org/0000-0001-9184-0897.

Әділет Мұхитұлы Сүгірбай – PhD, конструкторлық бюро жетекшісі, Ветеринария және ауыл шаруашылығы зерттеу мектебі, Шәкәрім Университеті, Қазақстан Республикасы; e-mail: Adilet_s_93@mail.ru. ORCID: https://orcid.org/0000-0003-3637-2749.

Сведения об авторах

Амангелді Булатұлы Шаяхметов – кандидат технических наук, ассоциированный профессор кафедры агроинженерии, механики и металлообработки, Казахский агротехнический исследовательский университет имени С.Сейфуллина, Республика Казахстан; e-mail: Shayahmetov0501@mail.ru. ORCID: https://orcid.org/0000-0001-9610-2631.

Татьяна Витальевна Бедыч* – кандидат технических наук, ассоциированный профессор кафедры энергетики и машиностроения, Костанайский инженерно-экономический университет им. М. Дулатова, Республика Казахстан; e-mail: tbedych@mail.ru. ORCID: https://orcid.org/0000-0003-3642-8917.

Максат Амантайулы Амантаев – PhD, ассоциированный профессор кафедры аграрной техники и транспорта, Костанайский региональный университет имени Ахмет Байтұрсынұлы, Республика Казахстан; e-mail: amantayev.ma@ksu.edu.kz. ORCID: https://orcid.org/0000-0002-4838-9487.

Риза Ғабдысалық – PhD, ассоциированный профессор сектора «Postgraduate», Восточно-Казахстанский технический университет им. Д. Серикбаева, Республика Казахстан; e-mail: riza.gabdyssalyk@mail.ru. ORCID: https://orcid.org/0000-0001-9184-0897.

Адилет Мухитович Сугирбай – PhD, руководитель конструкторского бюро, Исследовательская школа ветеринарии и сельского хозяйства, Шәкәрім университет, Республика Казахстан; e-mail: Adilet_s_93@mail.ru. ORCID: https://orcid.org/0000-0003-3637-2749.

Received 16.07.2026
Revised 04.09.2026
Accepted 07.09.2026

https://doi.org/10.53360/2788-7995-2026-3(23)-33

IRSTI: 53.49.37

CC BY 4.0
Check for updates

A. Kusainov, G. Zhunissova*, N. Magazov, A. Kengesbekov, L. Bayatanova
D. Serikbayev East Kazakhstan Technical University,
070004, Kazakhstan , Ust-Kamenogorsk, Serikbayev str. 19
*e-mail: junusova6@gmail.com

THE EFFECT OF ELECTROLYTE-PLASMA HARDENING PARAMETERS ON THE MICROSTRUCTURE, PHASE COMPOSITION, AND MECHANICAL AND TRIBOLOGICAL PROPERTIES OF 20X STEEL

Abstract: *This article investigates the effect of electrolytic-plasma treatment (EPT) parameters–voltage (260-320 V) and dwell time (2-5 s) – on the microstructure, phase composition, microhardness, elastic modulus, and tribological properties of 20X steel. Treatment was performed in a 12 wt.% Na_2CO_3 aqueous solution. X-ray diffraction and scanning electron microscopy showed the formation of α'-martensite with a body-centered cubic (BCC) lattice without residual austenite or carbide phases. The threshold treatment mode was 260 V for 2 s, at which complete austenitization was not achieved. Increasing the dwell time to 5 s at 300 V nearly doubled the microhardness to 441.66 HV, while increasing voltage at 2 s primarily affected carbon*

©A. Kusainov, G. Zhunissova, N. Magazov, A. Kengesbekov, L. Bayatanova, 2026

supersaturation. The lowest friction coefficient (μ = 0.498) was obtained at 320 V for 2 s, indicating that maximum hardness does not necessarily correspond to the best tribological performance. The results demonstrate that EPT parameters should be selected according to the required operational properties of 20X steel.

Key words: *electrolytic plasma treatment; 20X steel; martensite; microhardness; phase composition; X-ray diffraction analysis; coefficient of friction; surface hardening.*

Introduction

Extending the service life of machine parts under severe wear, contact loads, and aggressive environments is a priority in modern mechanical engineering. A large share of component failures stems from degradation of the surface layer, which bears the brunt of mechanical and tribological stress [1], making targeted modification of its structure and properties increasingly important.

Among surface-hardening approaches, coating methods (CVD/PVD, gas-thermal spraying, chromium electroplating) are most widespread and provide high hardness and wear resistance. However, coatings are dissimilar from the base metal, producing residual interfacial stresses and reduced adhesive strength under cyclic and impact loads [2]; most coating technologies also require costly vacuum equipment, high temperatures, and toxic reagents, limiting mass-production use.

An alternative to coatings is thermal/thermochemical treatment, where hardening occurs through structural and phase transformations within the workpiece itself, without a foreign layer. Electrolytic plasma treatment (EPT) heats the surface via electrical discharges in a vapor-gas envelope formed when the part is immersed in an electrolyte under high voltage (typically 200–400 V). High power density in the discharge zone heats the surface to austenitizing temperature within a fraction of a second; cooling on removal from the electrolyte or power-off then produces a martensitic transformation. Because the hardened layer is an integral part of the workpiece, EPT avoids delamination and gives a gradient property transition to the core, while offering simple equipment, environmentally safe aqueous electrolytes, and high productivity, with processing times of seconds to tens of seconds [3, 4].

20X chromium-alloyed structural steel was selected for this study, as it is widely used for gears, shafts, bushings, and other wear- and load-bearing components [6]. Its chromium content (0.7-1.0 wt.%) provides good hardenability and a tendency toward fine-grained martensite on quenching, making it promising for EPT-based surface hardening [5, 7].

Despite growing interest in EPT of various steels and alloys [1, 3, 4, 6, 7], systematic data on how voltage and holding time affect the structural, mechanical, and tribological properties of 20X steel remain scarce. In particular, the threshold parameters for complete martensitic transformation, the relationship between XRD-determined crystal-structure parameters and service characteristics, and optimal processing conditions for chromium-containing steels are not yet established – questions with both scientific and practical significance for the technology's industrial application.

The objective of this work is to investigate the effect of stress and holding time during electrolytic plasma treatment on the phase composition, microstructure, microhardness, and elastic modulus of the surface layer of 20X steel, as well as to evaluate the tribological characteristics – specifically, the coefficient of friction and the geometric parameters of wear tracks – and to establish correlations between the structural changes identified by X-ray diffraction and scanning electron microscopy, and the mechanical properties of the treated surface layer.

Materials and Methods

Alloyed structural steel 20X was used as the test material. The chemical composition of the steel is given in Table 1. The specimens were rectangular plates measuring 30×25 mm and 20 mm thick, ground by hand sequentially on sandpaper with grit sizes ranging from P100 to P2500.

Table 1 – Chemical Composition of 20X Steel (GOST 4543-2016) [9], wt.%

C	Si	Mn	Cr	Ni	S	P	Cu	Fe
0.17-0.23	0.17-0.37	0.50-0.80	0.70-1.00	≤0.30	≤0.035	≤0.035	≤0.30	base

Electrolytic plasma treatment was performed on an EPT laboratory setup equipped with a control unit capable of regulating voltage and treatment time (Fig. 1). The setup includes a conical stainless-steel electrolytic cell, an electrolyte circulation system with a pump, and an electrolyte bath. The sample (anode) was placed in the electrolyte flow at a fixed distance from the cathode; a stainless steel cell served as the cathode.

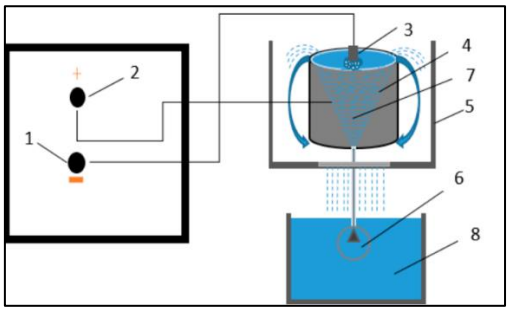


Figure 1 – Schematic of the EPT setup:
1 – anode; 2 – cathode; 3 – workpiece (sample); 4 – conical stainless steel electrolytic cell; 5 – sedimentation tank; 6 – pump; 7 – electrolyte; 8 – electrolytic bath

An aqueous solution of soda ash (Na_2CO_3) with a concentration of 12 wt.% (88 wt.% distilled water) was used as the electrolyte. The electrolyte circulated in the electrolytic cell via a pump with a flow rate of 60 L/min, ensuring uniform washing of the cathode located inside the cell. Through the upper opening of the cell, the electrolyte returns to the settling tank, passing close to the surface of the workpiece (anode). When an electrical voltage is applied between the anode and cathode, electrolyte ions such as H^+, OH^-, and CO_3^{2-} begin to move in an orderly fashion, causing the anode and the adjacent layer of electrolyte to heat up rapidly and form a vapor-gas envelope. As a result, the ionized electrolyte vapor forms an environment in which electrical discharges occur between the electrolyte and the anode, and the temperature of the sample gradually increases.

A uniform electrolyte composition (12% Na_2CO_3) was used under the voltage/time conditions listed in Table 2 to evaluate their effect on 20X steel properties.

Table 2 — Electrolyte-plasma treatment conditions for 20X steel samples

№	1	2	3	4	5	6
Voltage, V	320	300	280	260	300	300
Time, s	2	2	2	2	3	5

The microhardness of the surface layer was determined by the Vickers method on a semi-automatic HVS-1MDT-AXY tester at a load of 0.05 kgf, averaging at least five measurements per sample.

The elastic modulus was evaluated using a FISCHER-SCOPE HM 2000 system (Helmut Fischer GmbH, Sindelfingen, Germany; WIN-HCU software v7.1) in accordance with ISO 14577 [13] on sample cross-sections, with load increased to 10 mN over 20 s and a 5 s dwell time at final load.

Tribological tests were performed on an Anton Paar TRb3 tribometer (Anton-Paar, Buchs, Switzerland) in a «ball-on-disc» configuration per ASTM G133-95 and ASTM G99 [11, 12], at room temperature without lubricant, using a 100Cr6 counterbody ball (6 mm radius). Test conditions were: 6 N load, 3 cm/s linear speed, 3 mm wear radius, 40 m total distance.

X-ray diffraction (XRD) analysis of the surface layer was performed on a DW_XRD_27MINI diffractometer using Cu Kα radiation (λ = 1.5406 Å) in the angle range 2θ = 20-90°, with a scan step of 0.02°, with an exposure time of 0.5 s per step. Phase identification was performed using the PDF-2 database; crystallite size was calculated using the Scherrer equation (K = 0.9). The crystal lattice parameter was determined from the position of the (110) reflection using the relationship $a = d(110)\cdot\sqrt{2}$. The microstructure of the cross-section and the morphology of the wear tracks and wear spots on the counterbody were examined using scanning electron microscopy (SEM) on a TESCAN VEGA4 LMH microscope (TESCAN, Czech Republic) at magnifications of ×500 and ×2000 in secondary electron mode (SE) mode. To reveal structural components, cross-sections of the samples were chemically etched with Nital, a solution of nitric acid (4 wt.%) in ethyl alcohol (96 wt.%), which selectively reveals ferrite, pearlite, martensite, and grain boundaries.

Results and Discussion

The results of the microhardness measurements are presented in Figure 2. The initial hardness of 20X steel in the normalized condition was 179.8 HV, which corresponds to typical values for the ferrite-pearlite structure of this steel grade.

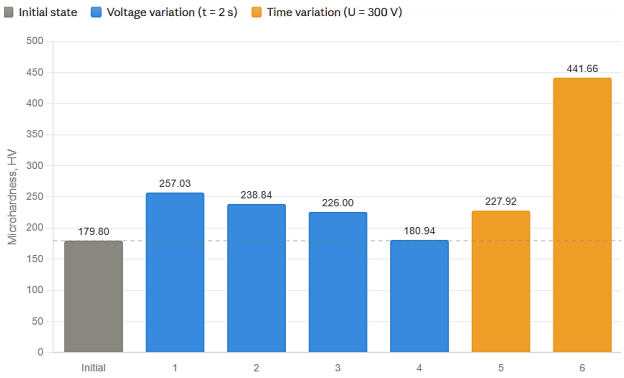


Figure 2 – Microhardness of the surface layer of 20X steel in the as-received condition and after EPT under various processing conditions

Analysis of the obtained data shows that microhardness of the 20X steel surface layer systematically increases with processing voltage at a constant holding time of 2 s. Reducing the voltage from 320 to 260 V causes an almost linear decrease in hardness from 257.03 to 180.94 HV, the latter being close to the initial value (179.8 HV), indicating insufficient process energy to form a hardened layer. Thus, 260 V at 2 s can be considered a threshold below which hardening is practically not realized.

At a constant voltage of 300 V, increasing the dwell time from 2 to 3 s causes no significant hardness change (238.84 and 227.92 HV), whereas increasing it to 5 s results in a sharp, nearly twofold increase to 441.66 HV. This nonlinear jump indicates a qualitative change in hardened layer formation in the 3-5 s range, which will be discussed based on SEM analysis.

Overall, holding time has a more pronounced effect on surface hardening of 20X steel than processing voltage, with a clear threshold and nonlinear character.

The elastic modulus results are shown in Figure 3. Except for 300 V/5 s, all EPT modes reduce the modulus from the initial 243.7 GPa. In the voltage series, it decreases to 197.5 GPa at 300 V and increases to 221.6 GPa at 260 V. With increasing hold time, it rises from 197.5 GPa (2 s) to 252.0 GPa (5 s).

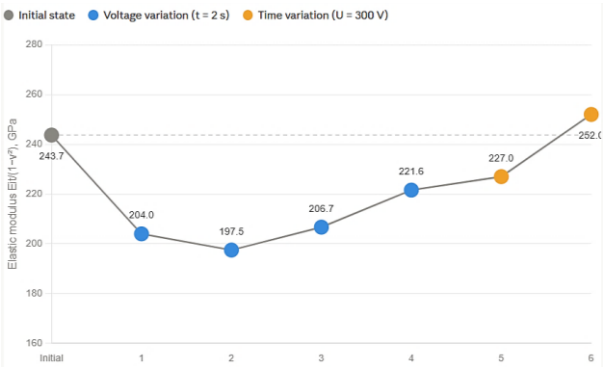


Figure 3 – Effect of electrolytic-plasma treatment conditions on the elastic modulus of the surface layer of 20X steel

The decrease is attributed to martensitic transformation, which increases hardness while moderately reducing the elastic modulus. The increase to 252.0 GPa in Mode No. 6 is associated with deeper martensitic transformation and a high-density dislocation substructure, confirmed by SEM and RSA.

Figure 4 shows the friction coefficient μ kinetics. All curves exhibit typical dry steel-on-steel sliding: a running-in stage (0-5 m), with μ increasing from zero to 0.40-0.55, followed by a quasi-steady increase. This behavior results from oxide film destruction and accumulation of tribochemical products. Average μ values for distances >5 m are given in Table 3.

At a constant exposure time of 2 s, decreasing the voltage from 320 to 260 V increases μ from 0.498 to 0.648. Only 320 V/2 s reduces μ below the untreated value (0.498 vs. 0.545), due to formation of a dense martensitic layer. At lower voltages, incomplete austenitization increases μ.

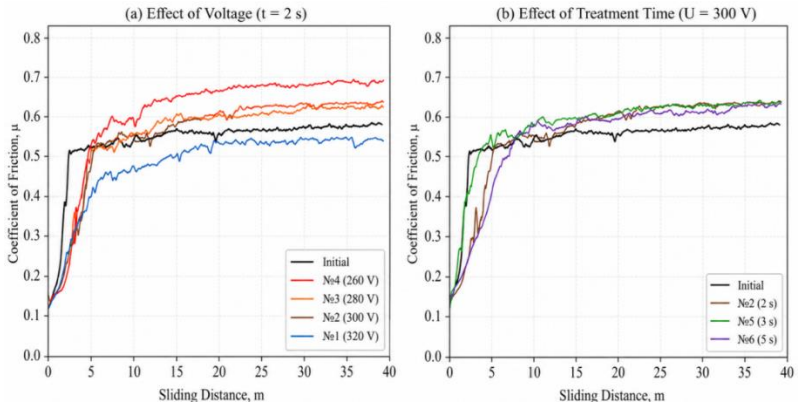


Figure 4 – Coefficient of friction of 20X steel as a function of sliding path:
a – effect of stress (t = 2 s); b – effect of holding time (U = 300 V)

Table 3 – Average values of the coefficient of friction for 20X steel in its as-received condition and after EPT

Sample	Mode	μ (average ± standard deviation)
Initial	–	0.545 ± 0.062
№ 1	320 V, 2 s	0.498 ± 0.072
№ 2	300 V, 2 s	0.588 ± 0.053
№ 3	280 V, 2 s	0.581 ± 0.075
№ 4	260 V, 2 s	0.648 ± 0.071
№ 5	300 V, 3 s	0.597 ± 0.050
№ 6	300 V, 5 s	0.580 ± 0.061

At 300 V, varying the holding time has a weaker effect, with μ ranging from 0.580-0.597. Sample No. 6, despite its maximum hardness of 441.66 HV, does not show the lowest μ, indicating no direct correlation between hardness and anti-friction properties.

Thus, Mode No. 1 (320 V, 2 s) is optimal, reducing μ from 0.545 to 0.498 and increasing microhardness from 179.8 to 257.0 HV. Wear-track morphology was further analyzed (Fig. 5) to clarify the wear mechanisms.

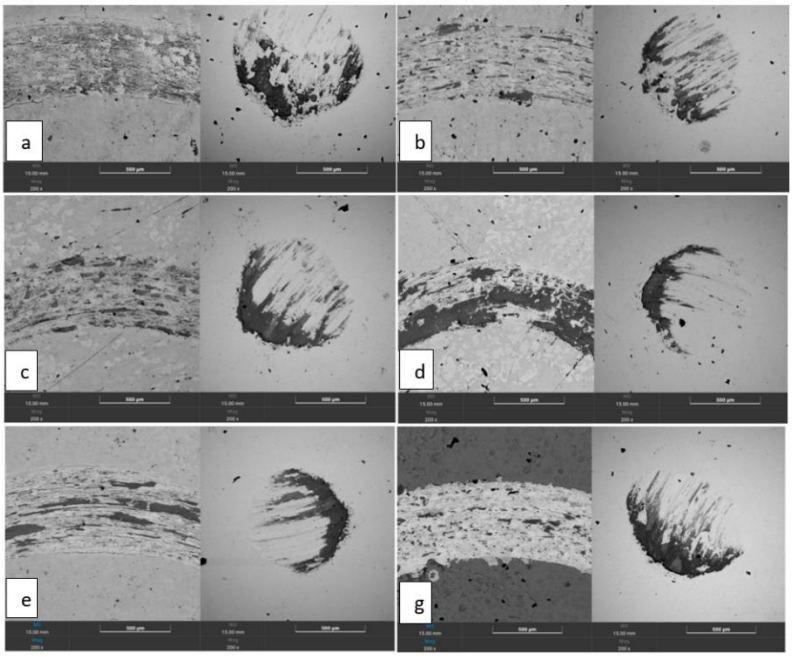


Figure 5 – Morphology of the friction surfaces of 20X steel after EPT:
a) Sample 1 (320 V, 2 s); b) Sample 2 (300 V, 2 s); c) Sample 3 (280 V, 2 s);
d) Sample 4 (260 V, 2 s); e) Sample 5 (300 V, 3 s); g) Sample 6 (300 V, 5 s)

Comparison of wear-track parameters with microhardness and friction coefficient shows no clear linear correlation between these characteristics.

Sample 4 had the narrowest wear track (458.54 μm), but hardness remained near the initial level (180.94 HV) and μ was maximum (0.648), indicating localized adhesive bonding rather than increased wear resistance. Sample No. 3 showed intermediate values: 226 HV, 501.99 μm, and μ = 0.581. Sample 6, despite maximum hardness (441.66 HV), had an intermediate track width (550.55 μm) and did not show the lowest μ, confirming that hardness does not directly determine friction. Sample 1 combined the lowest μ (0.498) with the largest wear track (561.49 μm) and ball wear spot (914.88 μm), indicating significant adhesive material transfer. The minimum counterface wear was observed for Sample 5 (607.42 μm), although its wear track was the widest (625.57 μm) (Table 4).

Table 4 – Geometric parameters of wear tracks and wear spots on the 20X steel counterbody after EPT, compared with microhardness and the coefficient of friction

Specimen	Conditions	Wear track width, μm	Ball wear spot width, μm	Microhardness, HV	Coefficient of friction, μ
Initial	–	443.77	761.01	179.8	0.545
№ 1	320 V, 2 s	561.49	914.88	257.03	0.498
№ 2	300 V, 2 s	540.48	696.07	238.84	0.588
№ 3	280 V, 2 s	501.99	696.22	226	0.581
№ 4	260 V, 2 s	458.54	723.15	180.94	0.648
№ 5	300 V, 3 s	625.57	607.42	227.92	0.597
№ 6	300 V, 5 s	550.55	756.88	441.66	0.580

Thus, friction, microhardness, and wear geometry are governed by different mechanisms and are not directly correlated. Microstructural and phase-composition analysis is therefore required. Cross-sections were metallographically examined after etching with 4 wt.% nitric acid in 96 wt.% ethyl alcohol to reveal ferrite, pearlite, martensite, and grain boundaries.

The as-received 20X steel (Fig. 6a) exhibits a homogeneous ferrite-pearlite structure without pronounced variation with depth. At ×2000 in SE mode, equiaxed ferrite grains with sharp boundaries and uniformly distributed fine pearlite colonies are observed. The uniform contrast indicates the absence of phases with significantly different atomic numbers, characteristic of normalized low-alloy structural steel.

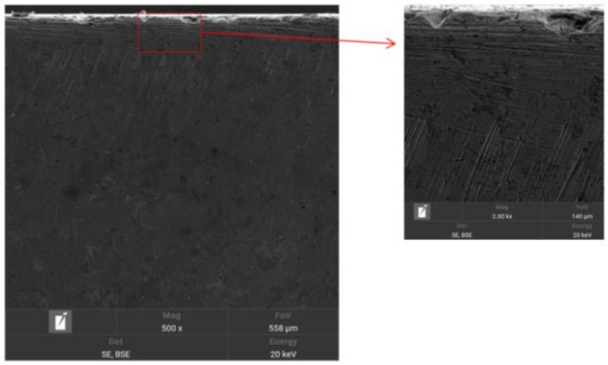


Figure 6a – Microstructure of 20X steel (initial state)

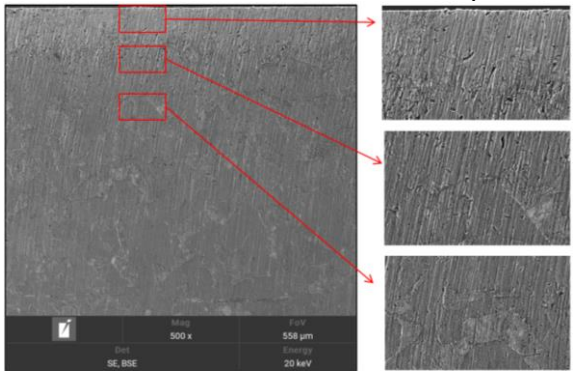


Figure 6b – Microstructure of 20X steel, sample No. 1 (320 V, 2 s)

After EPT in Mode No. 1 (320 V, 2 s), the cross-section (Fig. 6b) shows pronounced zonality. The near-surface zone (×2000, position 1) contains a fine needle-like structure oriented mainly perpendicular to the surface, characteristic of martensite formed by rapid heating to the austenitizing temperature and electrolyte quenching. The transition zone (position 2) contains martensitic regions and light-colored areas indicating incomplete austenitization. In the lower zone (position 3), the structure approaches the initial ferrite-pearlite state, confirming that EPT affects mainly the near-surface layer.

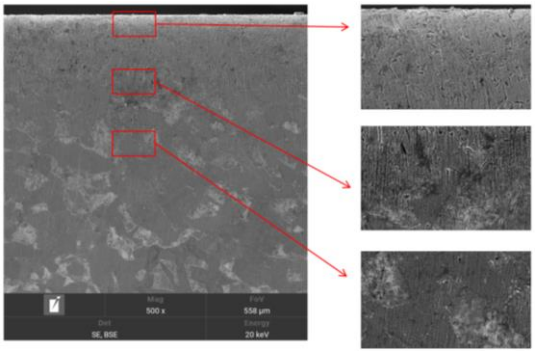


Figure 6c – Microstructure of 20X steel, specimen No. 4 (260 V, 2 s)

Specimen No. 4 (260 V, 2 s) shows no pronounced zonality at ×500 (Fig. 6c). At ×2000, the near-surface zone (position 1) exhibits a weak fine-grained relief, while positions 2 and 3 retain a ferrite-pearlite structure with partially coarsened grains. The absence of a pronounced martensitic layer agrees with the microhardness of 180.94 HV, confirming that 260 V for 2 s is insufficient for complete surface austenitization and martensitic transformation.

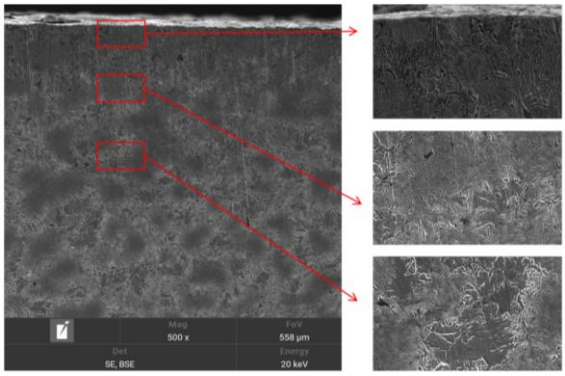


Figure 6d – Microstructure of 20X steel, sample No. 6 (300 V, 5 s)

The most significant structural changes were observed in Sample No. 6 (300 V, 5 s) (Fig. 6d). At ×500, a homogeneous fine-grained dark zone occupies the entire observed cross-section, while at ×2000, a well-developed needle- and plate-like martensitic structure extends throughout the section depth (at least 500 μm). Unlike Sample No. 1, where martensite is confined to the near-surface layer, Sample No. 6 shows deeper heating, explaining its maximum microhardness (441.66 HV). X-ray diffraction analysis was therefore performed to confirm these findings.

XRD was performed for the as-received sample and EPT Modes No. 1 (320 V, 2 s), No. 4 (260 V, 2 s), and No. 6 (300 V, 5 s). The diffractograms (Fig. 7) show (110), (200), and (211) α-Fe reflections with a BCC lattice. No residual austenite (γ-Fe) or Fe_3C reflections were detected. The absence of austenite confirms rapid electrolyte quenching and complete martensitic transformation under effective EPT conditions (Table 5).

In all treated samples, the surface layer consists exclusively of α′-martensite (BCC lattice), with (110), (200), and (211) α-Fe reflections identified; no retained austenite (γ-Fe) or Fe_3C reflections were detected, confirming a high electrolyte quenching rate. This is consistent with SEM data: Sample No. 1 shows fine-needle martensite near the surface, Sample No. 6 shows martensite throughout the section (≥500 μm), while Sample No. 4 lacks a continuous martensitic layer, matching its low hardness (180.94 HV).

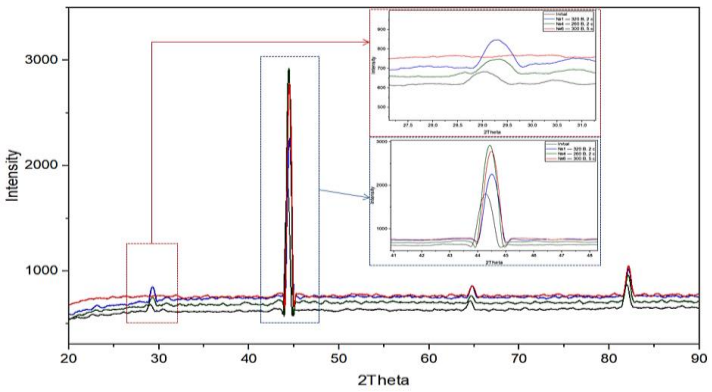


Figure 7 – Diffractograms of 20X steel in the as-received condition and after EPT:
a) full range 2θ = 20-90°; b) magnified fragment in the (110) reflection region

Table 5 – X-ray peak parameters and crystallite size determined by the Scherrer method for 20X steel

Sample	2θ, °	(hkl)	d, Å	FWHM, °	Iotn, %	D, nm
Initial	44.26	(110)	2.0464	0.1771	100	48.4
	64.69	(200)	1.4409	0.3542	4.3	26.5
	81.87	(211)	1.1767	0.1574	14.3	66.8
№ 1 (320 V, 2 s)	44.49	(110)	2.0365	0.1771	100	48.5
	64.73	(200)	1.4402	0.3936	4.9	23.9
	82.10	(211)	1.1740	0.1968	12.0	53.5
№ 4 (260 V, 2 s)	44.39	(110)	2.0406	0.1574	100	54.5
	64.68	(200)	1.4412	0.4723	1.9	19.9
	82.03	(211)	1.1747	0.1574	8.7	66.9
№ 6 (300 V, 5 s)	44.46	(110)	2.0379	0.1378	100	62.3
	64.81	(200)	1.4386	0.3149	3.1	29.9
	82.12	(211)	1.1737	0.1378	9.8	76.5

A weak oxide reflection (2θ ≈ 29.5°, presumably Fe_3O_4) appears in the initial sample and Mode No. 4, intensifies in Mode No. 1 (short 2 s exposure limits oxide removal), and disappears in Mode No. 6 (longer 5 s exposure restores the oxide layer). This oxide phase does not prevent Mode No. 1 from achieving the minimum friction coefficient (0.498), since the martensitic structure – not the oxide film – governs friction behavior.

The (110) reflection shifts to larger 2θ angles (44.26°→44.39–44.49°), corresponding to a decrease in lattice constant a from 2.894 Å to 2.880-2.886 Å. The largest shift occurs in Mode No. 1 (a = 2.880 Å), indicating maximum carbon supersaturation and explaining its best tribological performance (μ = 0.498). Mode No. 4 shows the smallest shift (a = 2.886 Å), consistent with threshold austenitization at 260 V, its highest friction coefficient (0.648), and lowest hardness.

Crystallite size D(110) increases from 48.4 nm (as-received) to 48.5 nm (No. 1), 54.5 nm (No. 4), and 62.3 nm (No. 6). Mode No. 1's minimal D(110) growth despite the largest lattice shift indicates fine-block, high-stress martensite that impedes plastic deformation and lowers μ. Mode No. 6's larger D(110) (62.3 nm) reflects coarsening from deep heating, explaining its maximum hardness (441.66 HV) but not improved friction, since coarser blocks reduce dislocation-barrier density.

Overall, RSA, SEM, microhardness, and tribological results agree: hardening and friction behavior depend jointly on martensitic transformation completeness, solid-solution supersaturation (a), and block size (D(110)). Mode No. 1 (320 V, 2 s) balances hardness (257.03 HV) and low friction (μ = 0.498) via fine-block martensite (a = 2.880 Å, D = 48.5 nm), while Mode No. 6 (300 V, 5 s) maximizes hardness (441.66 HV) through block coarsening (62.3 nm) without friction benefit – underscoring the need to select EPT modes based on the part's operational requirements.

Conclusion

A comprehensive study of the influence of electrolytic plasma treatment (EPT) parameters on the microstructure, phase composition, and mechanical and tribological properties of 20X steel revealed several patterns linking structural changes to the operational characteristics of the surface layer.

X-ray diffraction showed that, in all investigated modes, α′-martensite with a body-centered cubic (BCC) lattice forms in the surface layer with a complete absence of retained austenite and carbide phases, indicating a high electrolyte quenching rate that precludes reverse transformation and carbide precipitation. Metallographic examination confirmed the zonal nature of structural changes: at 320 V, 2 s, the martensitic zone is limited to the near-surface layer, whereas at 300 V, 5 s, it extends to a depth of at least 500 μm – directly reflected in this mode's maximum microhardness (441.66 HV). A voltage of 260 V with a 2 s hold time was established as the threshold below which complete austenitization is not achieved, evidenced by hardness at the initial-state level (180.94 HV), minimal shift of the (110) reflection (RSA data), and absence of a pronounced martensitic layer (SEM data). Increasing hold time at fixed voltage primarily governs the depth of the martensitic zone and crystallite size, while increasing voltage at fixed hold time affects carbon supersaturation of the solid solution, reflected in the lattice parameter.

The best anti-friction properties were achieved at 320 V, 2 s (μ = 0.498), due to fine-block, high-stress martensite with maximum lattice compression (a = 2.880 Å) and a high defect density that reduces adhesive interaction with the counterface. In contrast, the mode with maximum hardness (441.66 HV) did not yield a comparable friction reduction, since coarsening of martensitic blocks to 62.3 nm lowers the density of dislocation-slip barriers – confirming the absence of a direct correlation between hardness and friction behavior.

Thus, the optimal EPT regime for 20X steel depends on operational requirements: 320 V, 2 s is recommended for parts under intense sliding friction, while 300 V, 5 s suits parts subjected to high contact loads requiring maximum surface hardness.

References

1. Spectroscopic study of electrolytic-plasma discharge during hardening of 20GL steel and its effect on microstructure and mechanical properties / B. Rakhadilov et al // Crystals. – 2025. – Vol. 15, № 11. – Art. 976. https://doi.org/10.3390/cryst15110976.
2. Adhesion mechanisms, evaluation techniques and modeling strategies in PVD coatings: from fundamentals to data-driven design / S.G. Jan et al // Journal of Materials Research and Technology. – 2026. – Available online. https://doi.org/10.1016/j.jmrt.2026.01.234.
3. Influence of plasma electrolytic hardening modes on the structure and properties of 65G steel / B.K. Rakhadilov et al // Eurasian Journal of Physics and Functional Materials. – 2021. – Vol. 5, № 3. – P. 209-221. https://doi.org/10.32523/ejpfm.2021050306.
4. Investigation of changes in the structural-phase state and the efficiency of hardening of 30CrMnSiA steel by the method of electrolytic plasma thermocyclic surface treatment / D. Baizhan et al // Coatings. – 2022. – Vol. 12, № 11. – Art. 1696. https://doi.org/10.3390/coatings12111696.
5. Investigation of the effect of technological parameters of the electrolyte-plasma carburization method on the phase structure and mechanical properties of 20X structural steel / B. Rakhadilov et al // AIMS Materials Science. – 2023. – Vol. 10, № 5. – P. 934-947.
6. Experimental and mathematical modeling study of plasma electrolytic oxidation (PEO) for surface hardening of 20Ch steel / K. Kombayev et al // Materials. – 2024. – Vol. 17, № 24. – Art. 6043. https://doi.org/10.3390/ma17246043.
7. Effect of electrolytic-plasma hardening on the microstructure and tribological properties of low-alloy steels / B. Rakhadilov et al // Metals. – 2025. – Vol. 15, № 7. – Art. 698. https://doi.org/10.3390/met15070698.
8. The impact of technological parameters of electrolytic-plasma treatment on changes in the mechano-tribological properties of steel 45 / B. Rakhadilov et al // AIMS Materials Science. – 2024. – Vol. 11, № 4. – P. 666-683.
9. GOST 4543-2016. Metal products made of structural alloy steel. Specifications. – Moscow : Standartinform, 2017. – 31 p. (In Russian).
10. Effect of electropolishing on the microstructure and tribological properties of electrolyte-plasma borided layers on 30KhGSA steel / L. Sulyubayeva et al // Materials. – 2025. – Vol. 18, № 21. – Art. 4867. https://doi.org/10.3390/ma18214867.
11. ASTM G99-17. Standard test method for wear testing with a pin-on-disk apparatus. – West Conshohocken, PA: ASTM International, 2017.

12. ASTM G133-05(2016). Standard test method for linearly reciprocating ball-on-flat sliding wear. – West Conshohocken, PA: ASTM International, 2016.
13. ISO 14577-1:2015. Metallic materials – Instrumented indentation test for hardness and materials parameters – Part 1: Test method. – Geneva : International Organization for Standardization, 2015.

Funding Information

This article was prepared as part of the MNVO research grant project BR24992864 «Development of Equipment and Technologies for the Surface Treatment of Parts for the Metalworking Industry».

А. Кусайнов, Г. Жүнісова*, Н. Магазов, А. Кеңесбеков, Л. Баятанова
Д. Серікбаев атындағы Шығыс Қазақстан техникалық университеті,
070004, Қазақстан Республикасы, Өскемен қаласы, Серікбаев көшесі, 19
*e-mail: junusova6@gmail.com

20Х БОЛАТЫНЫҢ МИКРОҚҰРЫЛЫМЫНА, ФАЗАЛЫҚ ҚҰРАМЫНА ЖӘНЕ МЕХАНИКАЛЫҚ-ТРИБОЛОГИЯЛЫҚ ҚАСИЕТТЕРІНЕ ЭЛЕКТРОЛИТТІ-ПЛАЗМАЛЫҚ ШЫҢДАУ ПАРАМЕТРЛЕРІНІҢ ӘСЕР

Бұл мақалада электролит-плазмалық өңдеудің (ЭПӨ) параметрлерінің кернеу (260-320 В) және ұстау уақыты (2-5 с) – 20Х болатының микроқұрылымына, фазалық құрамына, микроқаттылығына, серпімділік модуліне және трибологиялық қасиеттеріне әсері зерттелген. Өңдеу концентрациясы 12 масс.% Na_2CO_3 сулы ерітіндісінде жүргізілді. Рентгендік дифракциялық талдау және растрлық электрондық микроскопия қалдық аустенит немесе карбидті фазалар болмаған кезде дене-центрленген текше (ДЦТ) торлы α'-мартенситтің түзілгенін көрсетті. Толық аустениттену қол жеткізілмеген шекті өңдеу режимі 260 В, 2 с болды. Ұстау уақытын 300 В кернеуде 5 с дейін ұлғайту микроқаттылықты 441,66 HV дейін екі есе дерлік арттырды, ал 2 с кезінде кернеуді арттыру негізінен көміртегінің қатты ерітіндіде қанығуына әсер етті. Ең төмен үйкеліс коэффициенті (μ = 0,498) 320 В, 2 с режимінде алынды, бұл максималды қаттылық әрдайым ең жақсы трибологиялық сипаттамаларға сәйкес келе бермейтінін көрсетеді. Алынған нәтижелер ЭПӨ параметрлерін 20Х болатының қажетті пайдалану қасиеттеріне сәйкес таңдау қажеттігін көрсетеді.

Түйін сөздер: *электролитті-плазмалық өңдеу; 20Х болаты; мартенсит; микроқаттылық; фазалық құрам; рентгендік дифракциялық талдау; үйкеліс коэффициенті; беткі қабатты шыңдау.*

А. Кусайнов, Г. Жүнісова*, Н. Магазов, А. Кеңесбеков, Л. Баятанова
Восточно-Казахстанский технический университет им. Д. Серикбаева,
070004, Казахстан , г. Усть-Каменогорск, ул. Серикбаева, 19
*e-mail: junusova6@gmail.com

ВЛИЯНИЕ ПАРАМЕТРОВ ЭЛЕКТРОЛИТНО-ПЛАЗМЕННОГО УПРОЧНЕНИЯ НА МИКРОСТРУКТУРУ, ФАЗОВЫЙ СОСТАВ И МЕХАНИЧЕСКИЕ И ТРИБОЛОГИЧЕСКИЕ СВОЙСТВА СТАЛИ 20Х

Данная статья исследует влияние параметров электролитно-плазменной обработки (ЭПО) напряжения (260-320 В) и времени выдержки (2-5 с) – на микроструктуру, фазовый состав, микротвёрдость, модуль упругости и трибологические свойства стали 20Х. Обработка проводилась в водном растворе Na_2CO_3 концентрацией 12 масс.%. Рентгеноструктурный анализ и растровая электронная микроскопия показали формирование α'-мартенсита с объёмно-центрированной кубической (ОЦК) решёткой без остаточного аустенита или карбидных фаз. Пороговым режимом обработки являлся режим 260 В при 2 с, при котором полная аустенитизация не достигалась. Увеличение времени выдержки до 5 с при 300 В почти удвоило микротвёрдость до 441,66 HV, тогда как повышение напряжения при 2 с преимущественно влияло на пересыщение твёрдого раствора углеродом. Минимальный коэффициент трения (μ = 0,498) был получен при 320 В в течение 2 с, что указывает на то, что максимальная твёрдость не всегда соответствует наилучшим трибологическим характеристикам. Полученные результаты демонстрируют, что параметры ЭПО должны подбираться в зависимости от требуемых эксплуатационных свойств стали 20Х.

Ключевые слова: *электролитно-плазменная обработка; сталь 20Х; мартенсит; микротвёрдость; фазовый состав; рентгенофазовый анализ; коэффициент трения; поверхностное упрочнение.*

Information about the authors

Arystanbek Kussainov – PhD doctoral student in Technical Physics, East Kazakhstan Technical University named after D. Serikbaev, Ust-Kamenogorsk, Kazakhstan; e-mail: arys20055@gmail.com. ORCID: https://orcid.org/0000-0003-4623-4681.

Gulnara Zhuniskyzy Zhunissova* – Master of Technical Physics, D. Serikbayev East Kazakhstan Technical University, Ust-Kamenogorsk, Kazakhstan; e-mail: junusova6@gmail.com. ORCID: https://orcid.org/0009-0008-2277-6666.

Nurtoleu Magazov – Researcher, Scientific Center «Protective and Functional Coatings», D. Serikbayev East Kazakhstan Technical University, Ust-Kamenogorsk, Kazakhstan; e-mail: magazovn@gmail.com. ORCID: https://orcid.org/0000-0002-9941-9199.

Aidar Kengesbekov – PhD, Leading Researcher at the Scientific Center «Protective and Functional Coatings» at the D.Serikbaev East State Technical University, Ust-Kamenogorsk, Kazakhstan; e-mail: kenesbekovaidar@gmail.com. ORCID: https://orcid.org/0000-0002-5630-9467.

Lyaila Bolatkanovna Bayatanova – PhD, Associate Professor at «D. Serikbayev East Kazakhstan Technical University» (“Center of Physics”), Ust-Kamenogorsk, Kazakhstan; e mail: leila_1809@mail.ru. ORCID: https://orcid.org/0000-0002-5630-4746.

Авторлар туралы мәліметтер

Арыстанбек Ерланович Кусайнов – «Техникалық физика» мамандығы бойынша докторант, Д. Серікбаев атындағы Шығыс Қазақстан техникалық университеті, Өскемен қ., Қазақстан; e-mail: arys20055@gmail.com. ORCID: https://orcid.org/0000-0003-4623-4681.

Гүлнара Жүнісқызы Жүнісова* – «Техникалық физика» мамандығы бойынша магистр, Д. Серікбаев атындағы Шығыс Қазақстан техникалық университеті, Өскемен қ., Қазақстан; e-mail: junusova6@gmail.com. ORCID: https://orcid.org/0009-0008-2277-6666.

Нуртолеу Магзумбекович Магазов – ғылыми қызметкер, «Қорғаныс және функционалдық жабындар» ғылыми орталығы, Д. Серікбаев атындағы Шығыс Қазақстан техникалық университеті, Өскемен қ., Қазақстан; e-mail: magazovn@gmail.com. ORCID: https://orcid.org/0000-0002-9941-9199.

Айдар Бақытбекұлы Кеңесбеков – PhD, Д. Серікбаев атындағы Шығыс Қазақстан техникалық университетінің «Қорғаныс және функционалдық жабындар» ғылыми орталығының жетекші ғылыми қызметкері, Өскемен қ., Қазақстан; e-mail: kenesbekovaidar@gmail.com. ORCID: https://orcid.org/0000-0002-5630-9467.

Ляйла Болатхановна Баятанова – PhD, қауымдастырылған профессор «Д. Серикбаев атындағы Шығыс Қазақстан техникалық университеті» («Физика орталығы»), Өскемен қ., Қазақстан; e-mail: leila_1809@mail.ru. ORCID https://orcid.org/0000-0002-5630-4746.

Сведения об авторах

Арыстанбек Ерланович Кусайнов – докторант по специальности «Техническая физика», Восточно-Казахстанский технический университет им. Д. Серикбаева, г. Усть-Каменогорск, Казахстан; e-mail: arys20055@gmail.com. ORCID: https://orcid.org/0000-0003-4623-4681.

Гүлнара Жүнісқызы Жүнісова* – магистр по специальности «Техническая физика», Восточно-Казахстанский технический университет им. Д. Серикбаева, г. Усть-Каменогорск, Казахстан; e-mail: junusova6@gmail.com. ORCID: https://orcid.org/0009-0008-2277-6666.

Нуртолеу Магзумбекович Магазов – научный сотрудник, Научный центр «Защитные и функциональные покрытия», Восточно-Казахстанский технический университет им. Д. Серикбаева, г. Усть-Каменогорск, Казахстан; e-mail: magazovn@gmail.com. ORCID: https://orcid.org/0000-0002-9941-9199.

Айдар Бақытбекұлы Кеңесбеков – PhD, ведущий научный сотрудник научного центра «Защитные и функциональные покрытия» в Восточно-Казахстанском техническом университете им. Д.Серикбаева, г. Усть-Каменогорск, Казахстан; e-mail: kenesbekovaidar@gmail.com. ORCID: https://orcid.org/0000-0002-5630-9467.

Ляйла Болатхановна Баятанова – PhD, ассоциированный профессор «Восточно-Казахстанского технического университета им. Д. Серикбаева» («Центр физики»), г. Усть-Каменогорск, Казахстан; e mail: leila_1809@mail.ru. ORCID: https://orcid.org/0000-0002-5630-4746.

Received 01.08.2026
Revised 02.09.2026
Accepted 08.09.2026